Aalto University

OPEN ACCESS

This is an electronic reprint of the original article.
This reprint may differ from the original in pagination and typographic detail.

Radfar, Behrad; Chen, Kexun; Setälä, Olli; Vähänissi, Ville; Savin, Hele; Liu, Xiaolong

Optoelectronic properties of black silicon fabricated by femtosecond laser in ambient air: exploring a large parameter space

Published in:
Optics Letters

DOI:
10.1364/OL.481890

Published: 01/03/2023

Document Version
Peer-reviewed accepted author manuscript, also known as Final accepted manuscript or Post-print

Please cite the original version:
Radfar, B., Chen, K., Setälä, O., Vähänissi, V., Savin, H., & Liu, X. (2023). Optoelectronic properties of black silicon fabricated by femtosecond laser in ambient air: exploring a large parameter space. *Optics Letters*, *48*(5), 1224 - 1227. https://doi.org/10.1364/OL.481890

This material is protected by copyright and other intellectual property rights, and duplication or sale of all or part of any of the repository collections is not permitted, except that material may be duplicated by you for your research use or educational purposes in electronic or print form. You must obtain permission for any other use. Electronic or print copies may not be offered, whether for sale or otherwise to anyone who is not an authorised user.

To be published in Optics Letters:

Title: Optoelectronic properties of black silicon fabricated by fs laser: Exploring a large parameter space

Authors: BEHRAD RADFAR,Kexun Chen,Olli Setälä,Ville Vähänissi,Hele Savin,Xiao-Long Liu

Accepted: 22 January 23

Posted 23 January 23

DOI: https://doi.org/10.1364/OL.481890

Published by Optica Publishing Group under the terms of the Creative Commons Attribution 4.0 License. Further distribution of this work must maintain attribution to the author(s) and the published article's title, journal citation, and DOI.

OPTICA PUBLISHING GROUP

Formerly OSA

Optoelectronic properties of black silicon fabricated by femtosecond laser in ambient air: Exploring a large parameter space

BEHRAD RADFAR, KEXUN CHEN, OLLI E. SETÄLÄ, VILLE VÄHÄNISSI, HELE SAVIN, XIAOLONG LIU*

Department of Electronics and Nanoengineering, Aalto University, Tietotie 3, FI-02150 Espoo, Finland
**Corresponding author: xiaolong.liu@aalto.fi*

Received XX Month XXXX; revised XX Month, XXXX; accepted XX Month XXXX; posted XX Month XXXX (Doc. ID XXXXX); published XX Month XXXX

We study the surface morphology, optical absorption (400–1100 nm) and carrier lifetime of black silicon fabricated by femtosecond (fs) laser in air. We explore a large laser parameter space for which we adapt a single parameter ξ to describe cumulative fluence delivered to the sample. We also study the laser-oxidized surface layer by measuring its photoluminescence spectra and comparing its effect on the aforementioned properties. Our study in a broad range of ξ is instructive in choosing laser parameters when targeting different applications. **© 2022 Optica Publishing Group**

OPTICA PUBLISHING GROUP
Formerly OSA

Femtosecond (fs) laser micromachining is a convenient technique to create surface textures that can effectively reduce reflection loss. The fs-laser micromachined silicon surface micro/nanostructures, or the so-called black silicon (bSi), are useful in many fields, such as photodetectors, solar cells, and functional surfaces [1]. Unlike other bSi texturing methods, such as metal-assisted chemical etching (MACE) or plasma etching, the fs-laser technique does not necessarily require poisonous gases or chemicals [2]. Also, patterning can be done directly without the need for photolithography steps [3]. However, typically the fs-laser has a markedly slow fabrication speed of ~1 cm^2/h to create structures with high light absorption, as most of the past works have used moderately low 1 kHz repetition rate pulses in line scan mode [4]. Nevertheless, there is great potential to improve the fabrication speed by using higher pulse energies and repetition rate [4,5] and/or by using advanced laser techniques such as beam shaping [6], multi-beams [7], and interference patterning [8].

A noteworthy benefit of laser micromachining is that the surface functionalization largely depends on the ambient during laser texturing [1,2]. In ambient air, for instance, an oxygen-rich surface layer can be formed by laser oxidation, which is known to show visible luminescence [9,10]. Besides, there are various laser parameters, including laser wavelength, pulse duration, repetition rate, fluence, focus area, scan speed etc., to vary even extensively [11], which means that the parameter space is large and there are numerous different combinations that could affect the surface characteristics. For a better depiction of the parameter choice, G. Nava et al. introduce an empirical 'figure of merit' ξ to describe the cumulative fluence delivered to the sample, which is correlated well with optical absorption [4]. This motivates us to see the correlation of absorption with other surface functions, taking luminescent structures into account (since it has been addressed rather separately from other properties [9,10]) under various laser parameters but simply described by a single parameter ξ.

On the other hand, electrical properties such as minority-carrier lifetime also play a vital role in photovoltaic devices, which has been far less considered in earlier studies on fs-laser textured bSi [11,12]. Specifically, there is no information on how carrier lifetime changes during the experimental migration to higher repetition rates or how the oxygen-rich layer could possibly affect carrier lifetime since it contains active recombination centers and might reduce the effectiveness of surface passivation. Considering all these material properties together could lead to the fact that different parameter combinations could prove out useful for various applications. This information is, however, not available since systematical studies of a large parameter space on these properties are so far missing.

In this paper, we aim for a comprehensive understanding of the fs-laser textured bSi processed in ambient air by examining the surface morphology, optical absorption, and minority carrier lifetime resulting from a wide range of parameter space. We also study the oxygen-rich layer by element analysis and spectral photoluminescence (PL) measurement and compare the effect of the existence of such layer on optical absorption and carrier lifetime of surface passivated bSi. Our variation in repetition rate and scan speed leads to a wide range of the parameter ξ that will help guide the choice of laser parameters when targeting various needs.

The starting wafers were 4" boron-doped FZ monocrystalline silicon with 3±2 Ω cm resistivity, 280 μm thickness and (100) orientation. In the beginning, the wafers were annealed in O_2 at 1050 °C for 30 min to passivate the bulk defects typically inherent in FZ wafers [13]. After the surface oxide layer was removed with a buffered HF solution and deionized water (DIW) rinse, wafers were quickly transferred to a laser

fabrication system. A Spectra-Physics Spirit 1040-16-SHG fs-laser was used to generate laser pulses with 520 nm wavelength, 324 fs pulse duration and a maximum power of ~11 W at 417 kHz repetition rate. The laser pulses were focused to a spot diameter of ~80 µm and a fluence of ~5.4 kJ/m^2 at the surface. The position and the scan speed of the laser were controlled by a galvoscanner, and raster scanning of the Si surface with 35 µm line spacing produced 1 cm^2 square areas in ambient air. An integrated pulse picker allowed reducing the repetition rate and average power. Two wafers with the same laser-processed regions were prepared in which the laser frequency and the scan speed were varied from 6.5 to 417 kHz and from 1 to 100 mm/s, respectively.

Laser-textured wafers were cleaned in a sequence of sonicated acetone, isopropanol and DIW rinse to remove laser-ablated debris. To remove the O-rich surface layer, one wafer was dipped in high-concentration HF (10%) solution for 5 min. For both as-lasered and HF (10%) dipped samples, Energy dispersive X-ray (EDX) analysis was performed with an FEI Helios Nanolab 600 DualBeam focused ion beam (FIB) system. Photoluminescence spectra (500–900 nm) were measured using a confocal microscopic system Witec Alpha 300, having an excitation wavelength of 402 nm and a power of 4 mW. The PL spectra were calibrated from the relative spectral response of the detection system.

Next, both wafers were cleaned with RCA-based procedures and transferred to a Beneq TFS-500 atomic layer deposition (ALD) system. Al_2O_3 with a thickness of ~50 nm was deposited on both sides of wafers using TMA and H_2O as precursors at 200 °C. As bare silicon surfaces contain large amount of defects including dangling bonds that are known to act as effective recombination sites, the ALD Al_2O_3 layer here serves as a surface passivation layer to reduce surface recombination [13,14]. Thus, double sided surface passivation allows us to study the minority carrier recombination inside silicon (and inside the bSi). Finally, the wafers were annealed in forming gas at 400 °C for 30 min to activate the surface passivation. The surface passivation quality of Al_2O_3 is strongly dependent on post-deposition annealing temperature, and 400 °C is a typical temperature to improve the interface quality between silicon and Al_2O_3 [14]. From these wafers, surface morphology was characterized with a Zeiss Supra 40 Field-Emission Scanning Electron Microscope (SEM) under various angles. Optical absorptance was measured by a Cary 5000 UV-Vis-NIR spectrophotometer with an integrating sphere. The minority carrier lifetime was measured by the contactless and nondestructive Microwave-detected PhotoConductance Decay (µ-PCD) method with a Semilab WT-85 wafer lifetime scanner. In this method, excess carriers are generated in silicon with a laser pulse, which changes the conductivity of the sample. Subsequently, time-dependent conductivity decay is monitored using reflected microwaves from the surface from which the minority carrier lifetime can be extracted [15].

Fig.1(a) shows the surface morphology of the textured areas with varied repetition rate and scan speed. Changing the repetition rate from 6.5 to 417 kHz at a fixed scan speed of 100 mm/s results in a drastic morphology change from nanoparticles to microcolumns. Owing to the surface textures, the optical absorptance shown in Fig.1(b) increases with increasing repetition rate, reaching >94% in a broad wavelength range from 400 to 1000 nm. At the maximum repetition rate of 417 kHz, the size of the surface textures further increases with decreasing scan speed, as seen in Fig.1(a), and the corresponding absorptance shown in Fig.1(c) also increases to >96% (from 400 to 1000 nm) at a speed of 40 mm/s. Although lower scan speed results in higher absorptance, we observe that the surface starts to melt at scan speed of 20 mm/s, and the wafer was even destroyed at lower speeds. This phenomenon arises from thermal accumulation effects [16] when there is insufficient time interval between pulses for localized heat to diffuse away.

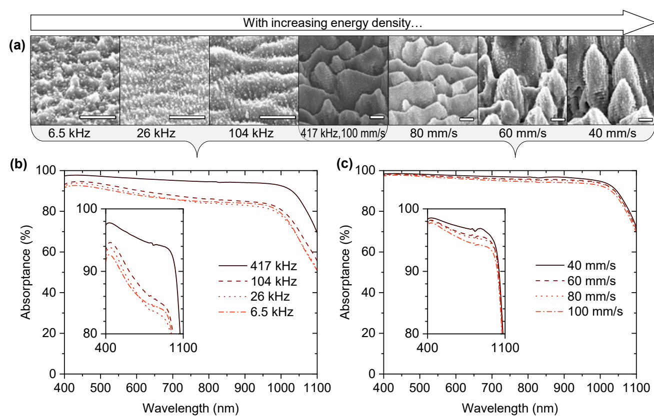

Fig. 1. (a) SEM images of fs-laser textured samples with varied repetition rate and scan speed, imaged viewed at 45° tilt and scale bar length 2 µm applied to all images. (b),(c) Optical absorptance of samples with (b) varied repetition rate at fixed 100 mm/s scan speed and (c) varied scan speed at fixed 417 kHz repetition rate. Insets are the same data shown with a narrower absorptance range (fluctuations after 800 nm are subject to detector change during measurements).

We define the parameter ξ (J/cm^2) as $\xi = \frac{\text{maximum laser power} \times \text{maximum repetition rate}}{\text{actual repetition rate} \times \text{scan speed} \times \text{line spacing}}$, which describes the cumulative laser energy density in a large area. It is a simplified version of the original definition proposed in Ref. [4] but will later prove useful for our study. As the ξ is proportional to the repetition rate and inversely proportional to scan speed, the increased morphological sizes and absorptance in Fig.1 can also be attributed to increased energy density. To keep the same ξ, we need to simultaneously vary both the repetition rate and scan speed. As shown in Fig.2, under the same ξ of 799 J/cm^2, all these parameters lead to similar high absorptance, but the highest repetition rate of 417 kHz still leads to slightly higher absorptance. To achieve higher ξ without melting the wafer at a high repetition rate, we use a combination of 52 kHz and 1 mm/s to demonstrate a much higher ξ of 4050 J/cm^2. Still, as seen in Fig.2, the resulting sample shows no improvement in the absorption. Therefore, there seems to be an optimal range of ξ for the highest absorptance; further increasing ξ may cause a more prominent particle or plasma shielding effect [17], which prevents the formation of effective light-trapping structures.

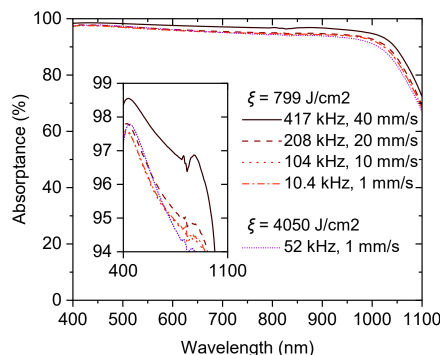

Fig. 2. Optical absorptance for samples with varied repetition rate and scan speed. Inset is the same data shown with a narrower absorptance range (fluctuations after 800 nm are subject to detector change during measurements).

In Fig.3(a), we observe that the surface of an as-lasered sample is covered by a mixed layer of oxygen and silicon, whereas a very low concentration of other possible elements (B from substrate doping, N and C from ambient air) is not detectable by EDX measurement. After dipping in HF (10%), the O elements cannot be differentiated from the background noise. The O-rich layer produced by laser oxidation affects the morphology and absorption in different ways. Fig.3(b) compares the change in morphology before and after HF dip, indicating the O-rich layer appears in the form of dendritic nanoclusters. Fig.3(c) compares the change in average absorptance before and after HF dipping as a function of the parameter *ξ*, repetition rate *f* and scan speed *v*. It appears that removing the O-rich layer decreases the absorption under lower *ξ* but increases absorption under higher *ξ*. Combining the morphologies observed in Fig.1(a) and Fig. 3(b), we conclude that under low ξ, the laser processing results in relatively small surface structures. When ξ is increased, small nanostructures start to form on top of the existing surface structures, which increases the effective surface area and thus results in increased absorption. When ξ is increased further, the surface structures become already microscopic in size decorated with nanosized structures increasing the surface area even more. However, in such large grooves, the O-rich structures backfill the grooves, reducing the antireflection effect. Therefore, a balanced parameter combination indicated by the dashed line, leads to the surface structure that is least affected by the laser-oxidized layer.

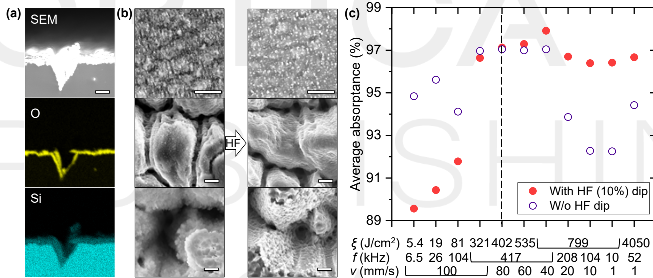

Fig. 3. (a) Cross-sectional SEM image of an as-lasered bSi sample (52 kHz and 1 mm/s) and corresponding EDX maps of O/Si elements. (b) Top view SEM images of fs-laser textured samples without (left column) and with (right column) HF (10%) dip. Used parameters from top to bottom: 26 kHz, 100mm/s; 417 kHz, 100 mm/s; 52 kHz and 1 mm/s. Scale bar length of 2 µm is applied to all images. (c) Average optical absorptance (400–700 nm) of all samples with a varied parameter *ξ*, repetition rate *f*, and scan speed *v*. Dashed line indicates the parameters where the absorptance is least affected by the oxygen-rich layer.

Fig.4 shows the measured PL signal of the as-laser textured black silicon. In Fig.4(a) and Fig.4(b), the PL intensity increases clearly with laser repetition rate and scan speed, respectively. In Fig.4(c), varying both repetition rate and scan speed shows random PL intensity, but the highest PL intensity is obtained with the highest *ξ* (marked with 52 kHz, 1 mm/s). As a reference, after dipping the same sample in HF the PL disappears, further proving that the PL signal comes from the O-rich layer. In Fig. 4(d), we summarize the average PL intensity from 500 to 900 nm as a function of the parameter *ξ*. A clear dependency of PL intensity on *ξ* can be observed. At a low ξ regime, increasing ξ leads to higher PL intensity suggesting higher laser energy leads to higher amount of luminescent structures on the bSi surface. At the same relatively high values of *ξ*, the different PL intensities may come from the fact that the surface morphology varies a lot, so the measured PL intensity is affected by the resulting average absorptance (see Fig.3(c)) and random angular distribution of luminescence. These results indicate that higher *ξ* is required to fabricate a high-efficiency luminescent structure which may find its place in, e.g., sensing applications [18].

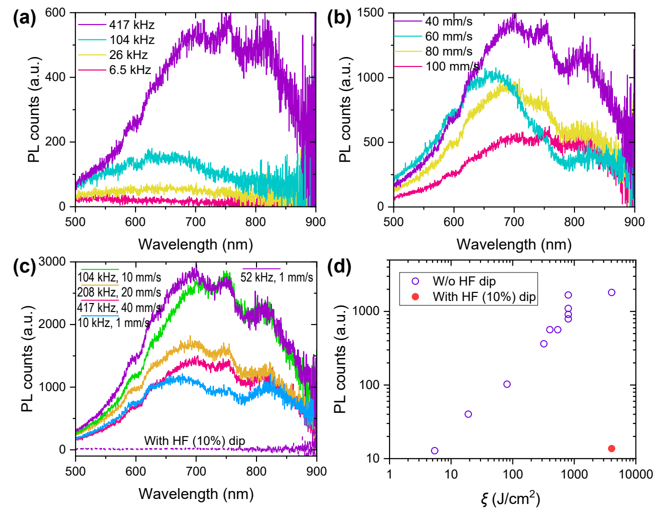

Fig. 4. (a)–(c) PL spectra of bSi samples fabricated from (a) varied repetition rate at fixed 100 mm/s scan speed, (b) varied scan speed at fixed 417 kHz repetition rate, (c) varied repetition rate and scan speed. All samples were characterized directly after laser processing except one reference sample that received 5 min HF (10%) dip. (d) Dependency of PL intensity (averaged from 500–900 nm) on the parameter *ξ*.

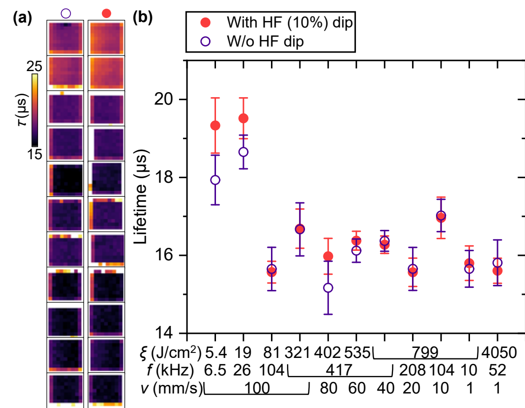

Fig. 5. (a) µPCD lifetime maps of laser-textured areas (1 cm × 1 cm) without (1st column) and with (2nd column) HF (10%) treatment. Color bar applies to all maps with white color indicating lifetime >25 µs and black <15 µs. (b) Average lifetime with standard deviation for each area shown in (a) from 100 pixels. Points from left to right correspond to maps from top to bottom.

As the O-rich layer is very much defective and relatively thick, it will prevent the underneath surface from being passivated and cause extra carrier recombination, which is detrimental for photovoltaic applications. In Fig.5, we present the minority carrier lifetime measurement from ALD Al_2O_3 surface passivated bSi samples with and without removing the O-rich layer. While minimal difference can be

OPTICA PUBLISHING GROUP
Formerly OSA

seen between samples with and without this O-rich layer in Fig.5(a), there are samples with specific laser parameters that clearly show a higher lifetime range. In Fig.5(b), we plot the average lifetime values from textured areas as a function of laser parameters. The lifetime saturates to around 16 μs already at a low ξ (81 J/cm^2) regime and the HF dip seems to cause no improvement in the lifetime. As a reference, the measured lifetime on our planar surface reaches as high as 3 ms. The results suggest that the lifetime is primarily limited by the bulk damage caused by the laser. At a lower ξ regime (<81 J/cm^2), the lifetime is slightly higher and removing the O-rich layer shows an apparent increase in lifetime, which indicates that the lower laser energy causes less bulk damage and this layer is indeed a source of recombination centers.

With the increasing parameter ξ, the cumulative effect of laser pulses on the silicon surface becomes more prominent. This accumulation of laser energy is essential when creating surface textures with effective light trapping. With carefully adjusted parameters, high optical absorptance can be easily achieved since it requires a relatively small ξ. Further increasing the absorptance is still possible by fine-tuning laser processing parameters, but this is beyond the scope of this study. To produce a more efficient luminescent structure, the suitable range of ξ is much higher than that for optimal absorption. There are many parameters that could lead to a higher ξ value, such as higher laser fluence, lower scan speed, higher repetition rate, smaller focus area, etc. However, in a higher ξ regime, the processing speed (scan speed) can be substantially low. In our experiment, texturing a 1 cm^2 area with 1 mm/s scan speed takes ~1 h. In contrast, with 417 kHz and 100 mm/s, it only takes <1 min to achieve similar high absorptance or PL intensity as compared to those obtained under lower repetition rates. Consequently, a high repetition rate is advantageous in fabricating high absorptance or high luminescence surface textures with shorter processing time which is preferred for large-scale production.

Although a smaller ξ value seems to lead to a higher lifetime (Fig.5), here we did not examine ξ <5.4 J/m^2 since there is a clear decrease in absorptance at lower ξ (Fig.3) and as a consequence, the sample is not 'black' anymore. Our previous study at a lower ξ regime (higher scan speed >100 mm/s at 417 kHz repetition rate) shows a clear trade-off between absorptance and lifetime [11]. Thus, further improvement of the lifetime for minority-carrier devices should rely on other post-laser processing treatments such as chemical etching [19]. It is worth mentioning that some other black silicon fabrication methods such as MACE and plasma etching cause much less bulk damage achieving ms-level lifetime combined with low reflectance [3]. On the other hand, inducing damage in crystalline material is a typical method to create a short carrier lifetime for high-speed detectors [20,21]. Therefore, combined high absorptance with low carrier lifetime demonstrated here may be suitable for high-speed silicon-based photodetectors if high photodetectivity is not necessary.

In summary, we have extensively examined the optical and electrical properties of the fs-laser textured black silicon processed in ambient air. A parameter ξ was adopted as a projection of all the used laser parameters. As ξ increased, the carrier lifetime first started to drop sharply and saturated to a minimum level. Then, absorption increased to a maximum level. Further increasing ξ led to stronger PL intensity originating from the surface O-rich layer. At the ξ regime, when absorption was maximized, such an O-rich layer showed the weakest effect on absorption and did not limit the carrier lifetime. Our study in a wide range of ξ values is instructive to retrodict the laser parameters when targeting different needs.

Funding. Business Finland (FemtoBlack, 7479/31/2019); Academy of Finland (NIR, 331313; PREIN, 320167); EMPIR programme co-financed by the Participating States and from the European Union's Horizon 2020 research and innovation programme (NanoWires, 19ENG05).

Acknowledgments. The authors acknowledge the provision of facilities and technical support by Micronova Nanofabrication Centre and Nanomicroscopy Centre in Espoo, Finland within the OtaNano research infrastructure at Aalto University. Lassi Hällström is acknowledged for the instruction on PL measurement.

Disclosures. The authors declare no conflicts of interest.

Data availability. Data underlying the results presented in this paper are not publicly available at this time but may be obtained from the authors upon reasonable request.

References

1. J.-H. Zhao, X.-B. Li, Q.-D. Chen, Z.-G. Chen, and H.-B. Sun, Mater. Today Nano **11**, 100078 (2020).
2. Z. Fan, D. Cui, Z. Zhang, Z. Zhao, H. Chen, Y. Fan, P. Li, Z. Zhang, C. Xue, and S. Yan, Nanomaterials **11**, 41 (2020).
3. X. Liu, B. Radfar, K. Chen, O. E. Setala, T. P. Pasanen, M. Yli-Koski, H. Savin, and V. Vahanissi, IEEE Trans. Semicond. Manuf. **35**, 504 (2022).
4. G. Nava, R. Osellame, R. Ramponi, and K. C. Vishnubhatla, Opt. Mater. Express **3**, 612 (2013).
5. K. Mishchik, G. Bonamis, J. Qiao, J. Lopez, E. Audouard, E. Mottay, C. Hönninger, and I. Manek-Hönninger, Opt. Lett. **44**, 2193 (2019).
6. N. Sanner, N. Huot, E. Audouard, C. Larat, and J.-P. Huignard, Opt. Lasers Eng. **45**, 737 (2007).
7. P. Hauschwitz, in *Laser Congress 2020 (ASSL, LAC)* (Optica Publishing Group, 2020), p. LW4B.3.
8. K. Cao, L. Chen, H. Wu, J. Liu, K. Cheng, Y. Li, Y. Xia, C. Feng, S. Zhang, D. Feng, Z. Sun, and T. Jia, Opt. Laser Technol. **131**, 106441 (2020).
9. T. Chen, J. Si, X. Hou, S. Kanehira, K. Miura, and K. Hirao, J. Appl. Phys. **110**, 073106 (2011).
10. A. V. Emelyanov, A. G. Kazanskii, M. V. Khenkin, P. A. Forsh, P. K. Kashkarov, M. Gecevicius, M. Beresna, and P. G. Kazansky, Appl. Phys. Lett. **101**, 081902 (2012).
11. X. Liu, B. Radfar, K. Chen, T. P. Pasanen, V. Vähänissi, and H. Savin, Adv. Photonics Res. **3**, 2100234 (2022).
12. S. S. Dissanayake, N. O. Pallat, P. K. Chow, S. Q. Lim, Y. Liu, Q. Yue, R. Fiutak, J. Mathews, J. S. Williams, J. M. Warrender, and M.-J. Sher, APL Mater. **10**, 111106 (2022).
13. J. Ott, T. P. Pasanen, P. Repo, H. Seppänen, V. Vähänissi, and H. Savin, Phys. status solidi **216**, 1900309 (2019).
14. G. Dingemans and W. M. M. Kessels, J. Vac. Sci. Technol. A Vacuum, Surfaces, Film. **30**, 040802 (2012).
15. M. Wilson, A. Savtchouk, J. Lagowski, K. Kis-Szabo, F. Korsos, A. Toth, R. Kopecek, and V. Mihailetchi, Energy Procedia **8**, 128 (2011).
16. I. Guk, G. Shandybina, and E. Yakovlev, Appl. Surf. Sci. **353**, 851 (2015).
17. E. Allahyari, J. JJ Nivas, M. Valadan, R. Fittipaldi, A. Vecchione, L. Parlato, R. Bruzzese, C. Altucci, and S. Amoruso, Appl. Surf. Sci. **488**, 128 (2019).
18. A. Y. Mironenko, M. V. Tutov, A. A. Sergeev, E. V. Mitsai, A. Y. Ustinov, A. Y. Zhizhchenko, D. P. Linklater, S. Y. Bratskaya, S. Juodkazis, and A. A. Kuchmizhak, ACS Sensors **4**, 2879 (2019).
19. X. Liu, B. Radfar, K. Chen, E. Palikko, T. P. Pasanen, V. Vahanissi, and H. Savin, IEEE Photonics Technol. Lett. **34**, 870 (2022).
20. N. K. Dutta, D. T. Nichols, D. C. Jacobson, and G. Livescu, Appl. Opt. **36**, 1180 (1997).
21. K. Preston, P. Dong, B. Schmidt, and M. Lipson, Appl. Phys. Lett. **92**, 151104 (2008).

Full reference list for review only

1. J.-H. Zhao, X.-B. Li, Q.-D. Chen, Z.-G. Chen, and H.-B. Sun. Ultrafast laser-induced black silicon, from micro-nanostructuring, infrared absorption mechanism, to high performance detecting devices. Mater. Today Nano **11**, 100078 (2020).
2. Z. Fan, D. Cui, Z. Zhang, Z. Zhao, H. Chen, Y. Fan, P. Li, Z. Zhang, C. Xue, and S. Yan. Recent Progress of Black Silicon: From Fabrications to Applications. Nanomaterials **11**, 41 (2020).
3. X. Liu, B. Radfar, K. Chen, O. E. Setala, T. P. Pasanen, M. Yli-Koski, H. Savin, and V. Vahanissi. Perspectives on Black Silicon in Semiconductor Manufacturing: Experimental Comparison of Plasma Etching, MACE, and Fs-Laser Etching. IEEE Trans. Semicond. Manuf. **35**, 504 (2022).
4. G. Nava, R. Osellame, R. Ramponi, and K. C. Vishnubhatla. Scaling of black silicon processing time by high repetition rate femtosecond lasers. Opt. Mater. Express **3**, 612 (2013).
5. K. Mishchik, G. Bonamis, J. Qiao, J. Lopez, E. Audouard, E. Mottay, C. Hönninger, and I. Manek-Hönninger. High-efficiency femtosecond ablation of silicon with GHz repetition rate laser source. Opt. Lett. **44**, 2193 (2019).
6. N. Sanner, N. Huot, E. Audouard, C. Larat, and J.-P. Huignard. Direct ultrafast laser micro-structuring of materials using programmable beam shaping. Opt. Lasers Eng. **45**, 737 (2007).
7. P. Hauschwitz. High-speed high-resolution multi-beam micromachining with ultrashort pulsed lasers, in *Laser Congress 2020 (ASSL, LAC)* (Optica Publishing Group, 2020), p. LW4B.3.
8. K. Cao, L. Chen, H. Wu, J. Liu, K. Cheng, Y. Li, Y. Xia, C. Feng, S. Zhang, D. Feng, Z. Sun, and T. Jia. Large-area commercial-grating-quality subwavelength periodic ripples on silicon efficiently fabricated by gentle ablation with femtosecond laser interference via two cylindrical lenses. Opt. Laser Technol. **131**, 106441 (2020).
9. T. Chen, J. Si, X. Hou, S. Kanehira, K. Miura, and K. Hirao. Luminescence of black silicon fabricated by high-repetition rate femtosecond laser pulses. J. Appl. Phys. **110**, 073106 (2011).
10. A. V. Emelyanov, A. G. Kazanskii, M. V. Khenkin, P. A. Forsh, P. K. Kashkarov, M. Gecevicius, M. Beresna, and P. G. Kazansky. Visible luminescence from hydrogenated amorphous silicon modified by femtosecond laser radiation. Appl. Phys. Lett. **101**, 081902 (2012).
11. X. Liu, B. Radfar, K. Chen, T. P. Pasanen, V. Vähänissi, and H. Savin. Tailoring Femtosecond-Laser Processed Black Silicon for Reduced Carrier Recombination Combined with >95% Above-Bandgap Absorption. Adv. Photonics Res. **3**, 2100234 (2022).
12. S. S. Dissanayake, N. O. Pallat, P. K. Chow, S. Q. Lim, Y. Liu, Q. Yue, R. Fiutak, J. Mathews, J. S. Williams, J. M. Warrender, and M.-J. Sher. Carrier lifetimes in gold–hyperdoped silicon—Influence of dopant incorporation methods and concentration profiles. APL Mater. **10**, 111106 (2022).
13. J. Ott, T. P. Pasanen, P. Repo, H. Seppänen, V. Vähänissi, and H. Savin. Passivation of Detector-Grade Float Zone Silicon with Atomic Layer Deposited Aluminum Oxide. Phys. status solidi **216**, 1900309 (2019).
14. G. Dingemans and W. M. M. Kessels, Status and prospects of Al_2O_3 -based surface passivation schemes for silicon solar cells. J. Vac. Sci. Technol. A Vacuum, Surfaces, Film. **30**, 040802 (2012).
15. M. Wilson, A. Savtchouk, J. Lagowski, K. Kis-Szabo, F. Korsos, A. Toth, R. Kopecek, and V. Mihailetchi. QSS-μPCD measurement of lifetime in silicon wafers: advantages and new applications. Energy Procedia **8**, 128 (2011).
16. I. Guk, G. Shandybina, and E. Yakovlev. Influence of accumulation effects on heating of silicon surface by femtosecond laser pulses. Appl. Surf. Sci. **353**, 851 (2015).
17. E. Allahyari, J. JJ Nivas, M. Valadan, R. Fittipaldi, A. Vecchione, L. Parlato, R. Bruzzese, C. Altucci, and S. Amoruso. Plume shielding effects in ultrafast laser surface texturing of silicon at high repetition rate in air. Appl. Surf. Sci. **488**, 128 (2019).
18. A. Y. Mironenko, M. V. Tutov, A. A. Sergeev, E. V. Mitsai, A. Y. Ustinov, A. Y. Zhizhchenko, D. P. Linklater, S. Y. Bratskaya, S. Juodkazis, and A. A. Kuchmizhak. Ultratrace Nitroaromatic Vapor Detection via Surface-Enhanced Fluorescence on Carbazole-Terminated Black Silicon. ACS Sensors **4**, 2879 (2019).
19. X. Liu, B. Radfar, K. Chen, E. Palikko, T. P. Pasanen, V. Vahanissi, and H. Savin. Millisecond-Level Minority Carrier Lifetime in Femtosecond Laser-Textured Black Silicon. IEEE Photonics Technol. Lett. **34**, 870 (2022).
20. N. K. Dutta, D. T. Nichols, D. C. Jacobson, and G. Livescu. Fabrication and performance characteristics of high-speed ion-implanted Si metal–semiconductor–metal photodetectors. Appl. Opt. **36**, 1180 (1997).
21. K. Preston, P. Dong, B. Schmidt, and M. Lipson. High-speed all-optical modulation using polycrystalline silicon microring resonators. Appl. Phys. Lett. **92**, 151104 (2008).